# Chapter 2

# The CDR method

## 2.1 Overview

The CDR method is based on the automated picking of pre-stack reflection seismic data (Riabinkin et al., 1962); the goal of this picking is to obtain the parameters of reflected waves. One of the picked parameters is traveltime (the time it takes a wave to travel from the source to the receiver). Another is ray parameter, defined as the change in traveltime as the position of the shot, receiver, or both, varies. The most useful ray parameters, for the purposes of tomographic velocity inversion, are the shot ray parameter (the change in traveltime as the shot position is varied, while the geophone position is held constant), and the geophone ray parameter (the change in traveltime as the geophone position is varied, while the shot position is held constant).

In the CDR method, the ray parameters are not determined by measuring the change in picked traveltime with respect to position ($\Delta t/\Delta x$). Instead, a gather of nearby traces is formed, and a slant stack is performed. The gather is thus transformed from $x$–$t$ to $p$–$\tau$ space, where $p$ is the ray parameter. On such a $p$–$\tau$ gather, the point of maximum amplitude is easily picked, and the position of this maximum gives the ray-parameter ($p$) and traveltime ($\tau$) information directly. Figure 2.1 shows how ray-parameter information (in this case, the geophone ray parameter) can be picked after slant stacking.

Note that the ray-parameter and traveltime information are easily picked by an automated algorithm. Since individual peaks are sought, rather than continuous horizons, the algorithm is comparatively simple. Note also that the CDR method is applied to pre-stack, unmigrated data.

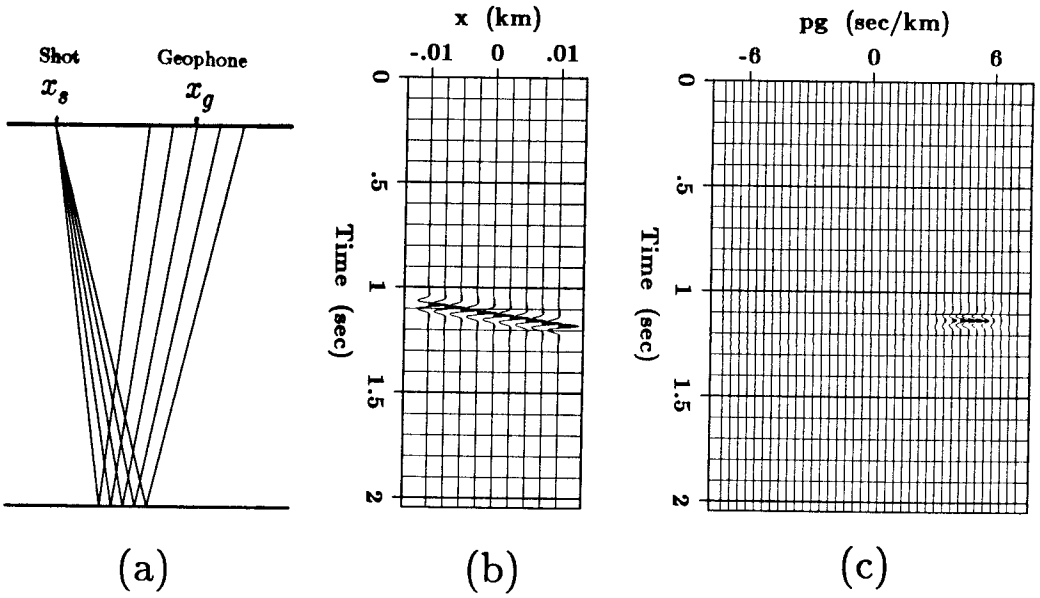


Figure 2.1: Determining ray parameters. Diagram (a) shows how a short-base common-shot gather might be collected in the field. Diagram (b) shows the outcome of this seismic experiment (notice that the horizontal coordinate in this diagram has its origin at location $x_g$). Diagram (c) shows the result of slant stacking this data; from the slant-stack section it is possible to determine the ray parameter $p_g$ (defined as $\Delta t/\Delta x_g$) and traveltime $t$ of the reflection event.

### 2.1.1 Reciprocal parameters

The ultimate goal of the CDR method as applied here is to determine the parameters of reflection events. Five parameters prove essential in CDR tomographic inversion: shot position $x_s$, geophone position $x_g$, shot ray parameter $p_s$, geophone ray parameter $p_g$, and traveltime $t$. Additional parameters such as amplitude, mean wavelength, and so on, can be picked as well, but these do not necessarily play a role in the inversion.

In Soviet geophysical terminology, approaches that use the shot and geophone ray parameters simultaneously are known as "reciprocal-point" methods. Thus, I shall refer to the five parameters $x_s$, $x_g$, $p_s$, $p_g$, and $t$, as the *reciprocal parameters*. Some overlap exists between the reciprocal-point and CDR methods, since the CDR method (meaning slant stacks plus picking) is often used to pick the reciprocal parameters. There are other techniques that can be used to determine these parameters, however. For instance, it is possible to perform a double slant stack to determine $p_s$ and $p_g$ simultaneously (Harlan and Burridge, 1983; Pan and Gardner, 1986). It is also possible to perform slant stacks over

midpoint and offset rather than over shot and geophone coordinates. In one technique, not directly related to CDR, information from a zero-offset section and from a conventional velocity analysis is used to find the five reciprocal parameters ($x_s$, $x_g$, $p_s$, $p_g$, $t$) that are used in the tomographic approach (Glogovskii et al., 1979).

### 2.1.2 Velocity and displays

Once the five reciprocal parameters have been found (picked), they can be used to determine an effective velocity (Puzyrev, 1979; Urupov and Levin, 1985), similar in concept to rms velocity (the similarities and differences are discussed in section 2.3.2, page 23). Each set of reciprocal parameters contains enough information to determine an effective velocity. Thus, each set of reciprocal parameters will have an effective velocity associated with it. The effective velocities can be used with the reciprocal parameters to produce a rough migrated section, even before the exact interval velocity structure has been determined. This migrated section will not look like a conventional migrated section; it will be a dip-bar section (a picture made up of short dipping line segments). Stereo display techniques can be used to produce 3-dimensional displays of the migrated data, where the two "flat" dimensions are the conventional midpoint and traveltime, while the third dimension, into the plane of the display, represents effective velocity. Such a stereoscopic display makes it easier for the interpreter to distinguish low-velocity phenomena (multiples, for instance) from high-velocity phenomena (primaries).

### 2.1.3 Velocity filtering

The effective velocities can also be used in velocity filtering. For example, all water-velocity events below the depth of the sea floor—such as water-bottom multiples—can be filtered out. Such velocity filtering is necessary, since CDR tomographic inversion is unable to distinguish between primary reflections and multiples. To achieve an accurate velocity inversion, it is necessary to eliminate all sets of reciprocal parameters associated with multiple reflections.

### 2.1.4 Previous work

Most of the material in this chapter is based on ideas developed over the last several decades in the U.S.S.R. It is likely that most or all of the equations in this chapter have

been previously published in the Soviet geophysical literature. Many of these equations do not appear in the most recent literature, however, and I have not conducted an extensive search of the older Soviet geophysical publications where they probably do appear. If an equation in this chapter is unreferenced, this means that I have rederived it myself, but I will not claim that I am the first to publish it. Judging by the level of development of the CDR method in the U.S.S.R., it is fair to assume that any such claim would be false.

I will, however, make two claims of originality in this chapter. As far as I have been able to determine, the stereo display of dip bars (Figures 2.8 and 2.9) has not been previously described. The picking techniques presented in Appendix A also make use of some original approaches. These approaches were not previously used because they are practical only on a large, powerful computer.

## 2.2 CDR picking methods

One goal of the CDR method is to determine three basic parameters for each reflection event in the seismic data: shot ray parameter ($p_s$), geophone ray parameter ($p_g$), and traveltime ($t$). Two other parameters are obtained directly from the geometry of the seismic survey: shot position ($x_s$), and geophone position ($x_g$).

These five parameters can be determined using the "classical" CDR approach (Riabinkin et al., 1962): slant stack over a gather of several traces, and pick peaks (maxima or minima). I will call this approach a *direct* picking method. Several *indirect*, non-CDR, picking methods exist as well.

### 2.2.1 Direct picking methods

The parameters $p_s$ and $p_g$ can be picked directly, or they can be derived from other, related information (information obtained by slant stacking common-offset and common-midpoint gathers, for instance). If a preliminary normal-moveout correction is applied to the data, the picked data are less likely to be aliased.

#### Picking $p_s$ and $p_g$

In the simplest form of direct picking, the parameters $p_s$ and $p_g$ (the shot and geophone ray parameters, respectively) are picked from the slant-stacked data. More specifically, suppose it is desired to determine the ray parameters of a reflected wave that has traveled

from shot location $x_s$ to receiver location $x_g$. To determine $p_g$, a gather is formed that contains all the traces that were recorded by receivers at or near position $x_g$, when the shot was fixed at position $x_s$. A slant stack is then performed over this gather. Similarly, to determine $p_s$, a gather is formed that contains all traces recorded at the fixed geophone position $x_g$, when the shot was at or near location $x_s$, and this gather is slant stacked.

The slant-stacking operation can be put in mathematical terms. Let the entire recorded wave field be described by $u_{ij}(t)$, where $i = 1, 2, 3..., n_{\text{shot}}$, and $j = 1, 2, 3..., n_{\text{geo}}$. Here $i$ is the shot location number, $j$ is the geophone location number, $n_{\text{shot}}$ is the number of shots, and $n_{\text{geo}}$ is the number of geophones. Suppose that the distance between shots is $\Delta s$, and the distance between geophones is $\Delta g$. Suppose, furthermore, that $n_{\text{base}}$ traces are to be added together to form the slant stack. Typical values of $n_{\text{base}}$ range from 7 to 15. The greater the value of $n_{\text{base}}$, the higher the signal-to-noise ratio of the slant stack, and the greater the resolution in $p$, but the lower the spatial resolution: the resolution cannot be better than $n_{\text{base}}\Delta s$ or $n_{\text{base}}\Delta g$.

The slant-stacked wave field $r_{g(m)}(t)$, used to find $p_g$, is produced according to the formula

$$r_{g(m)}(t) = \sum_{k=-n_{\text{bh}}}^{n_{\text{bh}}} u_{i(j+k)}(t + mk\,\Delta p\,\Delta g), \tag{2.1}$$

where $i$ is the shot index, $j$ is the geophone index, $m$ depends on the ray parameter $p_g$ according to the formula $p_g = m\,\Delta p$, and $n_{\text{bh}} = (n_{\text{base}} - 1)/2$. The other variables are as previously defined. Figure 2.1 shows the results of carrying out such a slant stack. One comment on notation: the symbol $\tau$, rather than $t$, is typically used to denote traveltime after slant stacking. I will not follow this convention, since it would lead to a certain amount of inconvenience, without increasing clarity. I will use $t$ to denote time both before and after slant stack.

Slant-stack peaks can be made sharper by applying semblance weighting to the slant stack (Kong et al., 1985; Stoffa et al., 1981). This semblance weighting is most effective when there is only one dip present at a particular time. The semblance weighting function $w_m(t)$ is

$$w_m(t) = \frac{\left[\sum_{k=-n_{\text{bh}}}^{n_{\text{bh}}} u_{i(j+k)}(t + mk\,\Delta p\,\Delta g)\right]^2}{(2n_{\text{bh}} + 1)\sum_{k=-n_{\text{bh}}}^{n_{\text{bh}}} u^2_{i(j+k)}(t + mk\,\Delta p\,\Delta g)}. \tag{2.2}$$

It is useful to smooth this weighting function in time, before applying it to the slant stack. If $w'_m(t)$ is defined to be the smoothed version of $w_m(t)$, then the slant stack $r_{g(m)}(t)$ is weighted according to

$$r_{g(m)}(t) = w'_m(t) \cdot r'_{g(m)}(t), \tag{2.3}$$

where $r'_{g(m)}(t)$ is the original unweighted slant stack. I use a 21-point time-domain boxcar smoothing function. Although I smooth the semblance $w_m(t)$, it may be better to smooth the numerator and denominator of equation (2.2) separately.

Equations (2.1) and (2.2) define the slant-stacking and semblance procedures when $u_{ij}$ is a continuous function of time. In practice, $u_{ij}$ is discretized in time, as is the output, $r_{g(m)}$. An interpolation scheme must be used to go from discretized to continuous time. The issue of interpolation is discussed in Appendix A, as are the criteria for choosing $\Delta p$, the discretization step of the ray parameter.

The slant-stack wave field $r_{s(m)}(t)$, used for finding $p_s$, is produced in a similar way to $r_{g(m)}(t)$:

$$r_{s(m)}(t) = \sum_{k=-n_{bh}}^{n_{bh}} u_{(i+k)j}(t + mk\,\Delta p\,\Delta s). \tag{2.4}$$

A semblance weight can be applied to $r_{s(m)}(t)$; the formulas, analogous to those in equations (2.2) and (2.3), will not be given here. Once the common-geophone and common-shot gathers have been transformed to the $r_{s(m)}(t)$ and $r_{g(m)}(t)$ slant-stack panels respectively, the picking process can begin. This process consists of looking for peaks (maxima and minima) on the slant-stack panels. A particular reflection event should have the same traveltime on both $r_{s(m)}(t)$ and $r_{g(m)}(t)$, since both panels are produced from gathers centered on the trace whose geophone is located at $x_g$ and whose shot is located at $x_s$. If peaks having identical traveltimes are found on both the $r_{s(m)}(t)$ and $r_{g(m)}(t)$ panels, it is likely that they correspond to the same event. I use a picking method loosely based on an algorithm developed in the Soviet Union (Rapoport, 1977). The details of the picking technique, including the process of correlation across the two slant-stack panels, are given in Appendix A.

### Determining $p_s$ and $p_g$ from $p_h$ and $p_y$

Depending on the recording geometry, it may be more convenient to pick data in common-midpoint and common-offset, rather than in common-shot and common-geophone coordinates. For example, land data, for which $\Delta s = \Delta g$ (shot spacing equals geophone

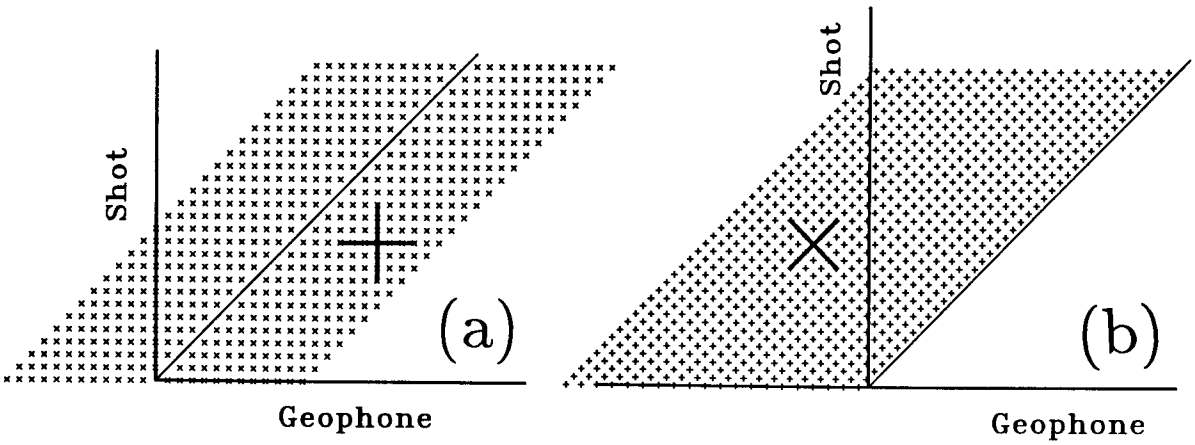


Figure 2.2: Picking $p_s$ and $p_g$ versus picking $p_y$ and $p_h$. Diagram (a) shows the stacking chart (the geometry of the observation system) for a typical land experiment, where $\Delta s = \Delta g$. The dots represent seismic traces, and the heavy lines represent the gathers over which slant stacking takes place to determine $p_s$ and $p_g$. Diagram (b) shows the stacking chart for a typical marine experiment, where $\Delta s = \Delta g/2$. In such an experiment, it is more convenient to form the gathers represented by the heavy lines and determine $p_y$ and $p_h$.

spacing), is most conveniently formed into common-shot and common-geophone gathers (Figure 2.2a). Accordingly, it is natural to slant stack these gathers to find $p_s$ and $p_g$. Marine data, on the other hand, is often recorded with the configuration $\Delta s = \Delta g/2$. Such data is most conveniently formed into common-offset and common-midpoint gathers (Figure 2.2b); these gathers can be slant-stacked and picked through a technique that is directly analogous to the previously described technique for determining $p_s$ and $p_g$.

In the notation used here, $h$, the half-offset, is defined by

$$h \equiv \tfrac{1}{2}(x_g - x_s), \tag{2.5}$$

while $y$, the midpoint, is defined by

$$y \equiv \tfrac{1}{2}(x_g + x_s), \tag{2.6}$$

where the shot and geophone positions are represented by $x_s$ and $x_g$, respectively. It is logical, then, to define $p_h$ as the change in traveltime with respect to offset (with midpoint fixed), and $p_y$ as the change in traveltime with respect to midpoint (with offset fixed).

Once $p_y$ and $p_h$ have been found from the slant-stacked midpoint and offset gathers, the corresponding values of $p_s$ and $p_g$ must be determined. The transformation is a simple

one. Recall that

$$p_s \equiv \frac{dt}{dx_s}, \qquad p_g \equiv \frac{dt}{dx_g},$$
$$p_h \equiv \frac{dt}{dh}, \qquad p_y \equiv \frac{dt}{dy}. \tag{2.7}$$

Then

$$p_s = \frac{dt}{dx_s} = \frac{dt}{dy}\frac{dy}{dx_s} + \frac{dt}{dh}\frac{dh}{dx_s} = \tfrac{1}{2}(p_y - p_h), \tag{2.8}$$

and

$$p_g = \frac{dt}{dx_g} = \frac{dt}{dy}\frac{dy}{dx_g} + \frac{dt}{dh}\frac{dh}{dx_g} = \tfrac{1}{2}(p_y + p_h). \tag{2.9}$$

Thus, equations (2.8) and (2.9) show how to determine $p_s$ and $p_g$, given $p_y$ and $p_h$.

As demonstrated in section 2.4, these picking techniques have been applied to a marine data set. The data were originally sampled with a geometry $\Delta s = \Delta g/4$, but I discarded every other shot profile, changing the geometry to $\Delta s = \Delta g/2$. I then picked $p_y$ and $p_h$ from the slant-stack panels, and transformed to $p_s$ and $p_g$.

### Determining $p_s$ and $p_g$ from moveout-corrected data

It is often helpful to apply a normal-moveout correction to the reflection seismic data before performing the slant stack (Riabinkin et al., 1962, p. 260). The normal-moveout correction reduces the apparent slope (ray parameter) of the far-offset data, thus lessening the risk of aliasing during the slant stack. In addition, the flattened data are more amenable to slant stacking, a process based on the assumption that traveltimes vary linearly, rather than hyperbolically, with horizontal position. The effects of the normal-moveout correction are removed when $p_s$, $p_g$, and $t$ are calculated, so it doesn't matter whether the moveout-correction velocity used is accurate or not.

Suppose that all traces have been moveout corrected at a constant velocity $v_0$. The moveout-corrected traveltime $t_{\mathrm{NMO}}$ can then be related to the old, uncorrected traveltime $t$ by the formula

$$t = \sqrt{t_{\mathrm{NMO}}^2 + \frac{4h^2}{v_0^2}}, \tag{2.10}$$

where $h$ is the half-offset, as defined in equation (2.5). Then, by equation (2.10) and the

definition of $p_s$,

$$p_s = \frac{dt}{dx_s} = \frac{1}{\sqrt{t_{NMO}^2 + \frac{4h^2}{v_0^2}}} \left( t_{NMO} \frac{dt_{NMO}}{dx_s} + \frac{4h}{v_0^2} \frac{dh}{dx_s} \right). \tag{2.11}$$

Let $p_{sNMO}$ be the measured change in moveout-corrected traveltime $t_{NMO}$ with respect to shot position, and let $p_{gNMO}$ be the corresponding change with respect to geophone position. By these definitions, equation (2.10), equation (2.11), and the definition of $h$,

$$p_s = \frac{1}{t} \left( t_{NMO}\, p_{sNMO} - \frac{2h}{v^2} \right). \tag{2.12}$$

Similarly, it can be shown that

$$p_g = \frac{1}{t} \left( t_{NMO}\, p_{gNMO} + \frac{2h}{v^2} \right). \tag{2.13}$$

Equations (2.10), (2.12), and (2.13) thereby show how $t_{NMO}$, $p_{sNMO}$, and $p_{gNMO}$, measured on moveout-corrected data, can be transformed to yield the parameters $t$, $p_s$, and $p_g$, just as if these parameters had been measured on data where the moveout correction was not applied. I used this transformation in determining the ray parameters for the marine data discussed in section 2.4; I chose a constant moveout-correction velocity of 1.6 km/sec.

### Two-way slant stacks

Other investigators (Harlan and Burridge, 1983; Pan and Gardner, 1986) have proposed a so-called "two-way" slant stack that allows $p_s$ and $p_g$ to be determined simultaneously, without the need to cross-correlate between two separate slant-stack panels. It combines, in effect, equations (2.1) and (2.4), producing as output a three-dimensional function in $p_s$, $p_g$, and $t$:

$$r_{mn}(t) = \sum_{k=-n_{bh}}^{n_{bh}} \sum_{l=-n_{bh}}^{n_{bh}} u_{(i+k)(j+l)}(t + mk\,\Delta p\,\Delta s + nl\,\Delta p\,\Delta g). \tag{2.14}$$

Here $m$ and $n$ specify the values $p_s = m\,\Delta p$ and $p_g = n\,\Delta p$. This three-dimensional space can be searched for maxima and minima; the position of an individual peak gives $p_s$, $p_g$, and $t$ directly.

One advantage of the two-way approach is that it makes use of more nearby traces in the slant stacking operation (see Figure 2.3); the signal/noise ratio is thereby increased. Another advantage of this approach is that $p_s$ and $p_g$ are picked simultaneously, eliminating the need for a cross-correlation step. Its main disadvantage is its heavy use of computer time.

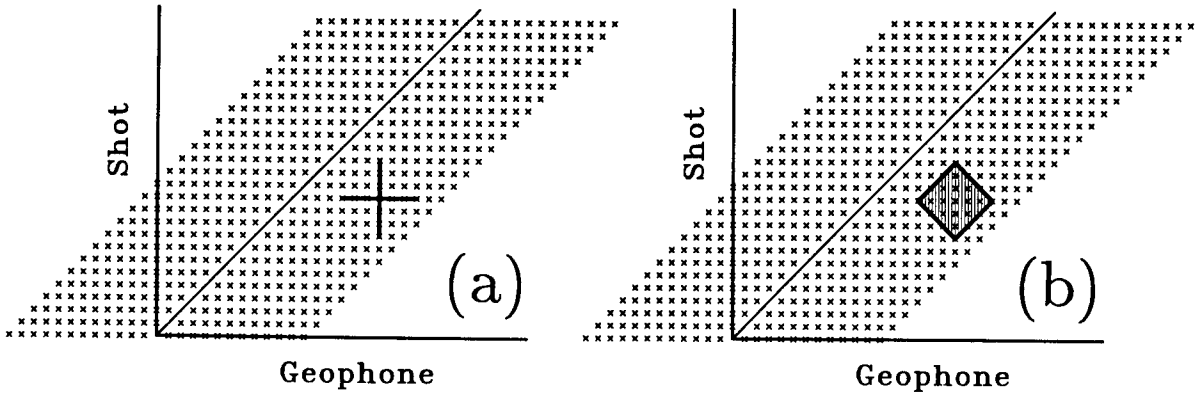


Figure 2.3: Two-way slant stacking. Diagram (a) shows a stacking chart from a typical land experiment, with heavy lines designating the gathers that are to be slant stacked to determine $p_s$ and $p_g$ (this is the same chart as in Figure 2.2a). Diagram (b) shows the same stacking chart, but now a hatched square shows all the gathers that are to be included in a two-way slant stack. The two-way slant stack is more expensive than the conventional slant stack, but it is more resistant to noise, since more gathers are used.

### 2.2.2 Indirect picking methods

It is sometimes better to determine the reciprocal parameters $x_s$, $x_g$, $p_s$, $p_g$, and $t$ from seismic data that has already been stacked. A primary reason for this would be the need to increase the signal/noise ratio. The main disadvantage of this approach is the implicit assumption that velocity does not vary quickly horizontally. I have not tested this approach myself, but I shall discuss it here because of its potential advantages.

#### Determining $p_s$ and $p_g$ from $t_0$, $p_{y_0}$, and $v$

It is possible to determine $p_s$ and $p_g$ indirectly, from parameters that at first glance do not contain the necessary information. Suppose that data have been collected using an off-end (non-symmetrical) geometry. Furthermore, suppose that the data for interpretation consist of a stacked (but unmigrated) section and the stacking velocity at each point. These data contain enough information to determine $p_s$ and $p_g$.

A gather is formed from the traces centered around the trace at midpoint $y_0$ on the stacked section. A slant stack is then performed on this gather, and peaks picked. If $p_{y_0}$ is defined as the change in simulated zero-offset traveltime with respect to midpoint $y$, then the picking yields $p_{y_0}$, as well as the simulated zero-offset traveltime $t_0$, at midpoint

$y_0$. (I use the word "simulated" to emphasize that these are not parameters taken from a true zero-offset section, but parameters taken from a stacked section, which is a simulated zero-offset section). It has been suggested (Will Gray, personal communication) that this picking step might be partially, rather than fully automated, allowing an interpreter to eliminate spurious picks caused by multiple reflections or noise. The inclusion of an interpreter is feasible, since slant stacks are performed on a single stacked section, rather than on a large pre-stack data set, as in the methods described previously.

Alternatively, $t_0(y)$ can be picked along a horizon. The $t_0$ values can then be smoothed, and $p_{y_0}$ determined explicitly from the formula $p_{y_0} = \Delta t_0/\Delta y$ (Glogovskii et al., 1979). If "bow ties" are present in the data, it may be difficult to pick the horizon $t_0(y)$. In such cases, a preliminary migration can be applied to the data to make the horizon more easily interpretable; the migrated horizon is picked, and then an inverse migration is applied to the picked horizon (Glogovskii et al., 1982). Such approaches are considered to fall within the method of reciprocal points, although they are not related to CDR.

Three other parameters besides $t_0$ and $p_{y_0}$ can be extracted from the stacked data set. One of these is $y_0$, the midpoint coordinate of the center trace in the slant-stacked gather. The second is $v_0$, the stacking velocity at midpoint $y_0$ and zero-offset traveltime $t_0$. The third, $h_{\mathrm{avg}}$, represents a simulated half-offset. That is, it represents the offset at which the parameters are supposed to have been measured. For the present, it is convenient to assume that if $h_{\mathrm{near}}$ is the near half-offset (that is, half the distance from the source to the nearest receiver), and $h_{\mathrm{far}}$ is the far half-offset, then $h_{\mathrm{avg}} = (h_{\mathrm{near}} + h_{\mathrm{far}})/2$. Note that $h_{\mathrm{near}}$ and $h_{\mathrm{far}}$ will probably vary with traveltime, depending on the muting scheme used. It is now clear why the original shooting geometry must be off-end: if the geophones are laid out symmetrically on both sides of the shot, then $h_{\mathrm{avg}} = 0$, which leads to many complications. (Split-spread data can still be used, of course, if the two sides of the spread are stacked separately.)

From the five parameters $t_0$, $p_{y_0}$, $h_{\mathrm{avg}}$, $y_0$, and $v_0$, it is possible to determine simulated values for the five reciprocal parameters $x_s$, $x_g$, $t$, $p_s$, and $p_g$; it may be helpful to smooth $v_0$ spatially before this determination is made (Glogovskii et al., 1979). The parameters $x_s$ and $x_g$ can be determined from $y_0$ and $h_{\mathrm{avg}}$, assuming that these latter two values follow the behavior of $h$ and $y$ in equations (2.5) and (2.6). Equations (2.5) and (2.6) are easily inverted to yield:

$$x_g = y_0 + h_{\mathrm{avg}}\,, \qquad x_s = y_0 - h_{\mathrm{avg}}\,. \tag{2.15}$$

The parameter $t$ can be determined:

$$t = \sqrt{t_0^2 + \frac{4h_{\text{avg}}^2}{v_0^2}}. \tag{2.16}$$

Then

$$p_s = \frac{dt}{dx_s} = \frac{1}{t}\left(t_0 \frac{dt_0}{dx_s} + 4\,\frac{h_{\text{avg}}}{v_0^2}\frac{dh_{\text{avg}}}{dx_s} - 4\,\frac{h_{\text{avg}}^2}{v_0^3}\frac{dv_0}{dx_s}\right). \tag{2.17}$$

Equation (2.16) is not strictly correct when velocity is allowed to vary spatially. It is therefore unclear whether the $dv_0/dx_s$ term in equation (2.17) is meaningful. For the sake of completeness I will retain terms of this type for the rest of the derivation; any reader who finds them objectionable is free to set them equal to zero.

From an equation analogous to equation (2.5), $dh_{\text{avg}}/dx_s = -1/2$. From the chain rule, the definition of $p_{y_0}$, and equation (2.6),

$$\frac{dt_0}{dx_s} = \frac{dt_0}{dy_0}\frac{dy_0}{dx_s} = \frac{p_{y_0}}{2}. \tag{2.18}$$

Similarly,

$$\frac{dv_0}{dx_s} = \frac{dv_0}{dy_0}\frac{dy_0}{dx_s} = \frac{1}{2}\frac{dv_0}{dy_0}. \tag{2.19}$$

Then, from equations (2.16), (2.17), (2.18), and (2.19),

$$p_s = \frac{1}{2t}\left(t_0 p_{y_0} - 4\,\frac{h_{\text{avg}}}{v_0^2} - 4\,\frac{h_{\text{avg}}^2}{v_0^3}\frac{dv_0}{dy_0}\right), \tag{2.20}$$

and

$$p_g = \frac{1}{2t}\left(t_0 p_{y_0} + 4\,\frac{h_{\text{avg}}}{v_0^2} - 4\,\frac{h_{\text{avg}}^2}{v_0^3}\frac{dv_0}{dy_0}\right). \tag{2.21}$$

Equations (2.20) and (2.21) were previously derived by Bandurin et al. (1982), in a slightly different form.

Equations (2.15), (2.16), (2.20) and (2.21) can thus be used to determine $x_s$, $x_g$, $p_s$, $p_g$, and $t$, once the parameters $y_0$, $h_{\text{avg}}$, $p_{y_0}$, $t_0$, and $v_0$ have been determined from the stacking velocity function, the stacked seismic data, and the recording geometry. This approach has been used in practice (Kopilevich et al., 1986). An important advantage of this approach, over the direct picking methods described previously, is that more traces are stacked together before the reciprocal parameters are chosen, thus making the reciprocal parameters more reliable. Another advantage, mentioned above, is that this method involves picking data from a relatively small data set (a stacked section), thus making it

feasible for a human operator to prevent bad picks from being made. The main disadvantage to this approach seems to be its lack of spatial resolution: the data are stacked over an entire range of offsets. Another disadvantage is that in regions with crossing dipping reflectors, the stacking velocity $v_0$ is, in theory, multivalued.

There exist a couple of useful tricks that help make this method more practical. Although $h_{\text{avg}}$ was defined previously to lie half-way between $h_{\text{near}}$ and $h_{\text{far}}$, it is actually possible to use an arbitrary value of $h_{\text{avg}}$ in the range $h_{\text{near}} \leq h_{\text{avg}} \leq h_{\text{far}}$. The reciprocal parameters, despite appearances, are only somewhat sensitive to the value of $h_{\text{avg}}$. In fact, several sets of reciprocal parameters can be picked at a single traveltime and midpoint, by plugging in different values of $h_{\text{avg}}$ into equations (2.15), (2.16), (2.20) and (2.21); this use of multiple $h_{\text{avg}}$ values can help increase the stability of the inversion (Glogovskii et al., 1979).

### Windowing over offset

One way to retain the advantages of the indirect method (the reduction of noise by stacking more data), while increasing the resolution, is to perform the preliminary stacking and velocity analysis over a narrower range of $h$ (half-offset) values. The transformation equations (equations (2.15), (2.16), (2.20), and (2.21)) remain valid; the only change is that $h_{\text{avg}}$ now represents the average offset over the offset window.

This idea can be combined with the two-way stack approach (defined in section 2.2.1 on page 15). A gather of traces, centered around a particular midpoint and offset, is formed. A slant stack over the midpoint coordinate is then carried out simultaneously with a velocity-analysis stack (a normal-moveout correction at various velocities, plus stack) over the offset coordinate (Kostov and Biondi, 1987). The result is a three-dimensional data volume with coordinates $v_0$, $p_{y_0}$, and $t$ (Urupov and Levin, 1985, pp. 172–174). Peaks can be picked from this volume, and the reciprocal parameters found according to the transformation equations given above.

### Data-determined $h_{\text{avg}}$

The resolution of the indirect method may be increased by allowing the data itself to determine the value of $h_{\text{avg}}$. One such approach has been developed by Will Gray (personal communication). During the regular processing sequence, a single trace is ordinarily formed on a stacked section by summing over a common-midpoint gather along hyperbolas

whose trajectories are determined by the stacking velocity. The stacking process will not be effective at all points along the hyperbolic trajectories, however. That is, the stacking will be effective when the hyperbolic trajectories are coincident with the hyperbolas on the common-midpoint gather, and will be ineffective otherwise. In general, the hyperbolic trajectories will be coincident with the hyperbolas in the data only at certain offsets (because of stacking-velocity errors, the presence of dipping reflectors, or non-hyperbolic moveout in the data). It is possible to perform partial stacks along the hyperbola, determine the offset where the stacking is most effective, and set $h_{\text{avg}}$ to be that offset.

### 2.2.3 Correlated CDR

A method known as Correlated CDR has recently been developed in the Soviet Union (Zavalishin, 1981). It is in some ways a hybrid between indirect and direct methods for determining $p_s$ and $p_g$. In this method, it is necessary only to know an approximate velocity, rather than an exact stacking velocity. Thus, it is better suited than indirect methods to regions with crossing dipping reflectors, since in such regions the stacking velocity can be multi-valued. I will not describe the Correlated CDR method here: its description is rather lengthy, and the main reference is already available in an English translation.

## 2.3 CDR migration, velocity analysis, and imaging

Once the reciprocal parameters, $x_s$, $x_g$, $p_s$, $p_g$, and $t$, have been determined, they can be used to construct migrated sections. An effective velocity can be determined for each set of parameters as well; this effective velocity is used in the migration (imaging) process and in velocity filtering. The methods that I describe in this section are not necessarily those that are used in the Soviet Union, but they produce similar results.

### 2.3.1 CDR constant-velocity depth migration

The reciprocal parameters can be used to produce constant-velocity migrated sections. The only difficulty in doing so is deciding which information to use. For example, suppose the five reciprocal parameters, $x_s$, $x_g$, $p_s$, $p_g$, and $t$, are known for a particular event; each of these parameters has some uncertainty associated with it. Suppose, in addition, that an a priori constant velocity is known (or guessed) for the medium. As shown in

section 2.3.2, the five reciprocal parameters are, by themselves, sufficient to determine the effective velocity of the medium, as well as the position and dip of the reflector. Thus, the a priori constant velocity adds redundant information. (This is *not* to say that the a priori information is unnecessary; it may be more reliable than some of the parameters.) The problem of finding the location and dip of the reflecting segment is now overdetermined.

The five reciprocal parameters are not all known to the same degree of accuracy. I consider the parameters $x_s$ and $x_g$ to be accurately known; they represent the physical position of the shot and geophone, so they are known within the precision of the land survey (others might argue that they are only known within an accuracy given by the spread lengths $n_{\text{base}}\Delta s$ and $n_{\text{base}}\Delta g$). I also find it reasonable to assume that the least accurately known parameters are the ray parameters $p_s$ and $p_g$. The parameter $t$, then, I consider to be of intermediate accuracy: the main errors in determining $t$ are caused by the length and phase characteristics of the source wavelet.

### Imaging the reflecting segment

If the shot and geophone positions, $x_s$ and $x_g$, are known, as are the a priori velocity $v$ and the traveltime $t$, then the reflecting segment must lie at a point $(y_R, z_R)$, somewhere along the ellipse described by the formula:

$$z_R^2 = \left(1 - \frac{4h^2}{v^2t^2}\right)\left(\frac{v^2t^2}{4} - (y_R - y)^2\right), \tag{2.22}$$

where $h$ and $y$ are defined according to equations (2.5) and (2.6). This ellipse is known as the "aplanatic surface" (Gardner, 1949).

Note that equation (2.22) was determined without any recourse to the ray parameters $p_s$ and $p_g$. These two parameters were intentionally excluded, since they are considered less reliable. They are used, however, to find the specific point on the ellipse where the reflecting segment lies. To accomplish this, $p_s$ and $p_g$ are first used to find the dip of the reflecting segment. In a constant-velocity medium, a ray traveling at an angle $\theta$ to the vertical has a ray parameter $p$, in accordance with the equation $\sin\theta = vp$. We can therefore speak of the shot ray traveling at an angle $\theta_s$, and the geophone ray traveling at an angle $\theta_g$, with these angles given according to the formulas

$$\begin{aligned} \sin\theta_s &= vp_s, \\ \sin\theta_g &= vp_g. \end{aligned} \tag{2.23}$$

Let the reflecting segment have a dip of angle $\phi$ (see Figure 1.1 on page 4 for a review of this notation). If Snell's law is assumed to hold, so that the angle of incidence of the shot ray equals the angle of reflection of the geophone ray, then it can be shown, after some algebra, that

$$\tan\phi = \frac{v(p_s + p_g)}{\sqrt{1 - v^2 p_s^2} + \sqrt{1 - v^2 p_g^2}}. \tag{2.24}$$

Once the dip angle $\phi$ is determined, it is possible to locate, on the ellipse described by equation (2.22), the point where a tangent line has the identical dip angle $\phi$. The reflecting segment must lie at this point. Equation (2.22) can be differentiated with respect to $y_R$, and the substitution $dz_R/dy_R = -\tan\phi$ made (the minus sign results because in this system of coordinates, $z_R$ increases with depth). Solving for $y_R$ thus yields the formula

$$y_R = y + \frac{\frac{vt}{2}\tan\phi}{\sqrt{1 - \frac{4h^2}{v^2t^2} + \tan^2\phi}}, \tag{2.25}$$

which gives the horizontal position, $y_R$, of the reflector, in terms of the five reciprocal parameters and the a priori velocity. Substituting this equation into equation (2.22) yields

$$z_R = \frac{\frac{vt}{2}\left(1 - \frac{4h^2}{v^2t^2}\right)}{\sqrt{1 - \frac{4h^2}{v^2t^2} + \tan^2\phi}}, \tag{2.26}$$

which gives the depth of the reflector.

Given the five reciprocal parameters and an a priori velocity, it is thus possible to use equations (2.24), (2.25), and (2.26) to find a dipping line, with dip angle $\phi$ and position $(y_R, z_R)$, corresponding to the dipping reflector that must have originally generated the reflection event. This dipping line (or dip bar) can be plotted, along with other dipping lines corresponding to other sets of reciprocal parameters, to give what is, in effect, a constant-velocity migrated depth section.

### The length of the reflecting segment

To construct a reasonable migrated depth section, it is necessary to know how long to draw the dipping lines that are supposed to represent the dipping reflectors. Typically, the length of the plotted dip bar is proportional to the resolution length of the reflecting

segment. Here, "resolution length" is understood to mean the shortest distance, along the reflector, for which a change in reflector characteristics can be resolved. This length can be estimated from the size of the Fresnel zone (Zavalishin, 1975). Such estimates show the resolution length to be proportional to the square root of depth. Other estimates of this length are based on the uncertainty in the ray parameter $p$ (Kozlov et al., 1975); these estimates show the resolution length to be directly proportional to depth. Depending on the dominant wavelength of the source wavelet, the width of the array over which slant stacking is performed, and the depth of the reflector, one or the other of these estimates may give the limiting resolution length (Phinney and Jurdy, 1979).

The question of reflector resolution is of interest to those who interpret the results of CDR migration, but it is not necessarily relevant to the problem of tomographic velocity estimation. As shown in Chapter 3, the estimated velocity structure is much more poorly resolved than are the reflectors; thus, it is not really important, from the point of view of velocity analysis, whether the reflector resolution varies directly or with the square root of depth. The plots in this chapter were made with dip bars whose length varies as the square root of depth. The dip-bar lengths are unrealistic, however, since in all cases they are less than the base length $n_{\text{base}}\Delta g$ (200 meters, for the data set used here).

### 2.3.2 CDR velocity analysis

The five reciprocal parameters, $x_s$, $x_g$, $p_s$, $p_g$, and $t$, are all that are needed to determine the velocity in the medium, if that velocity is assumed to be constant. The formula for determining this velocity is well-known in the Soviet Union; it was independently and simultaneously developed in about 1945 by three Soviet scientists: N.N. Puzyrev, Iu.V. Riznichenko, and V.N Rudnev (Urupov and Levin, 1985, p. 147). Most importantly, it is independent of the dip or curvature of the reflecting horizon (Puzyrev, 1979, p. 222; Goldin, 1986, p. 27). According to this formula,

$$v_{\text{CDR}}^2 = \frac{1 - \frac{h}{t}(p_s - p_g)}{(p_s - p_g)\frac{t}{4h} + p_s p_g}, \tag{2.27}$$

where $v_{\text{CDR}}$ is defined to be the velocity determined through use of the reciprocal parameters, and $h$ is as defined in equation (2.5). It should be noted that as $h$ approaches zero, this equation becomes more sensitive to errors in $p_s$ and $p_g$. On the other hand, it has been pointed out (Boris Zavalishin, personal communication) that as $h$ increases, one is

more likely to encounter other problems, such as refracted waves, anisotropy, and a lower signal/noise ratio.

The value $v_{\mathrm{CDR}}$ is an averaged velocity. It is analogous to average velocity, which is defined according to the formula

$$v_{\mathrm{avg}}(z) \equiv \frac{z}{\int_0^z 1/v(z')\,dz'}, \tag{2.28}$$

and root-mean-square velocity, which is defined according to the formula

$$v_{\mathrm{rms}}{}^2(z) \equiv \frac{\int_0^z v(z')\,dz'}{\int_0^z 1/v(z')\,dz'}, \tag{2.29}$$

where $v(z)$ is the interval velocity (Hubral and Krey, 1980, p. 16). The value $v_{\mathrm{CDR}}$ is known in Soviet seismological terminology as a "differential effective parameter" (Puzyrev, 1979). For flat layers, $v_{\mathrm{CDR}}$ approaches $v_{\mathrm{rms}}$ as offset $h$ approaches zero (Urupov and Levin, 1985, p. 103). As seen later in this chapter, $v_{\mathrm{CDR}}$ is used for velocity filtering and for producing certain kinds of plots. It is not, however, used directly in the process of tomographic velocity analysis that will be described in the next chapter.

### 2.3.3 CDR display techniques

One of the most interesting aspects of the CDR method is the speed and flexibility it allows in plotting the picked data. CDR data are quickly migrated, and they contain information not found in other representations of seismic data. For instance, a velocity, $v_{\mathrm{CDR}}$, can be associated with each dip bar. Examples of this flexibility in plotting will be shown below; the examples are based on picked marine seismic data (the data, from offshore Southern California, are provided courtesy of British Petroleum). Strong water-bottom multiples are evident in all the examples. The process of picking these data is described in section 2.2 and in Appendix A; Figures 2.10 and 2.11 (page 32) give an idea of how well the picking procedure worked.

#### CDR depth migration

Equations (2.24), (2.25), and (2.26) provide all the information necessary for constructing a constant-velocity depth-migrated section. Such a section is illustrated in Figure 2.4,

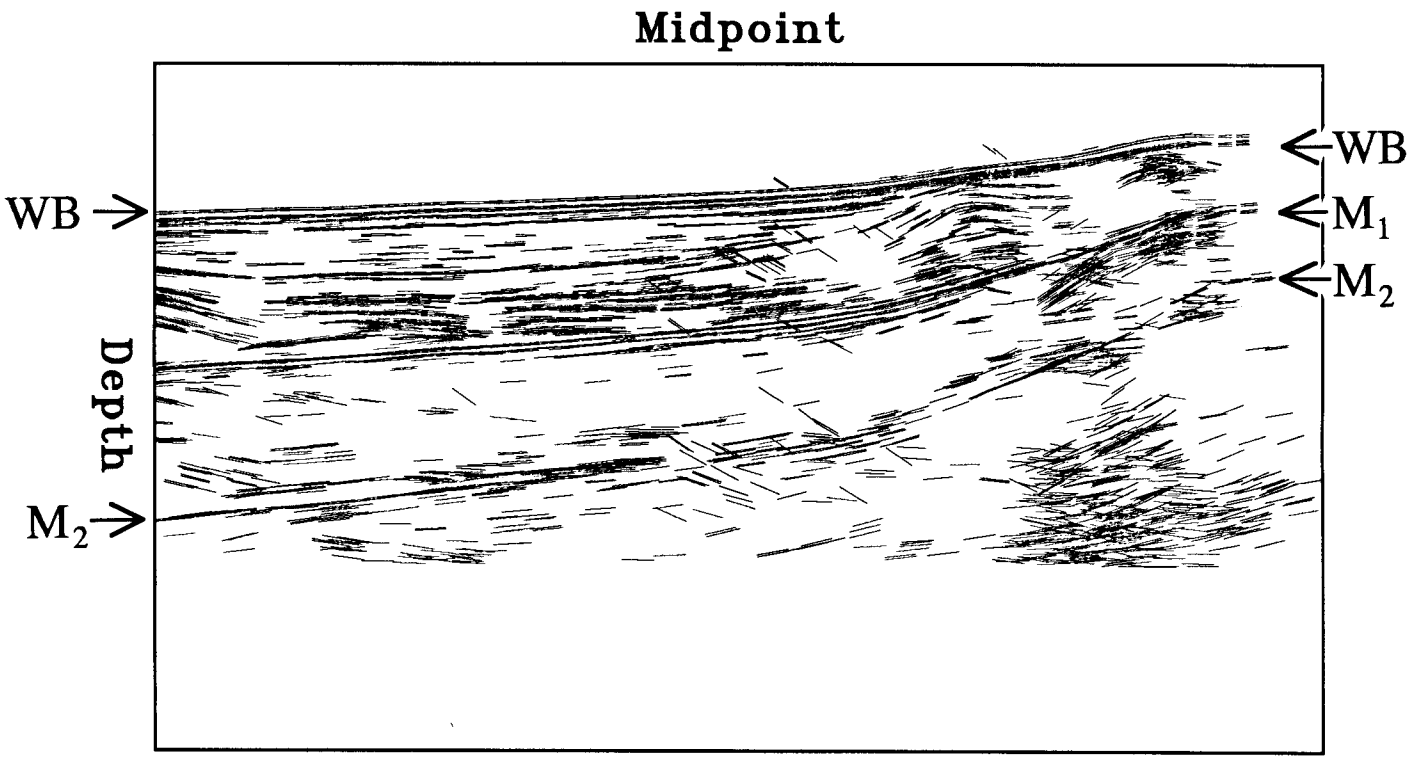


Figure 2.4: CDR migrated depth section. Marine data from offshore Southern California (courtesy of British Petroleum) were picked; the resulting reciprocal parameters were depth migrated as described in the text at a constant velocity of 1.48 km/sec (water velocity). Note that while the water-bottom reflection and multiples are well focused, the other events are fuzzy. Arrows WB, $M_1$, and $M_2$ point to the water-bottom reflection and the first and second multiples, respectively.

which is constructed assuming a constant velocity $v = 1.48$ km/sec (water velocity). Note that the water-bottom reflection and the water-bottom multiples are well focused; other reflectors appear fuzzier.

A different type of depth migration is possible when the velocity $v = v(x, z)$ is assumed to be known a priori. Ray-tracing techniques can then be used, for each set of reciprocal parameters, to determine the position of the associated reflecting segment. The difficulty is that, as in section 2.3.1 above, the problem is overdetermined. This aspect of depth migration will be discussed in section 3.5 (page 53).

### Taking advantage of $v_{\text{CDR}}$

The CDR velocity $v_{\text{CDR}}$ can be used in place of an a priori velocity (recall that each set of picked parameters has an associated $v_{\text{CDR}}$, determined according to equation (2.27)).

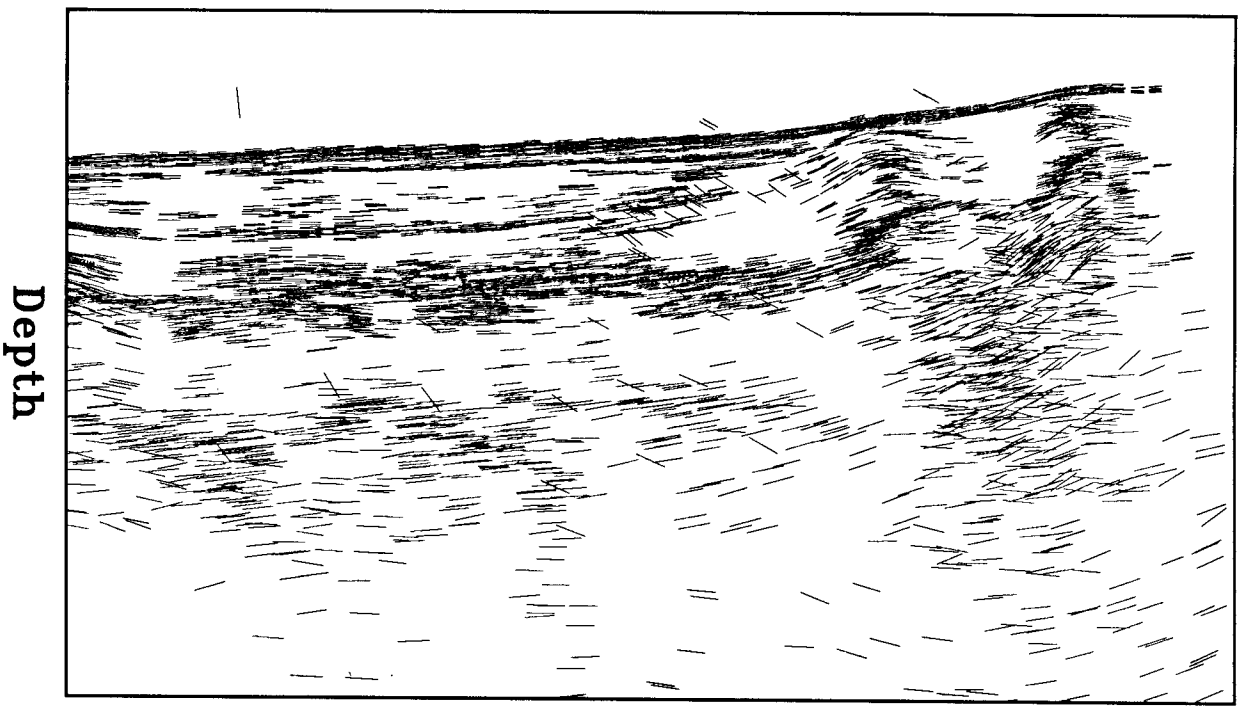


Figure 2.5: CDR migrated depth section ($v = v_{\mathrm{CDR}}$). The same picked parameters are used as were used to produce Figure 2.4, but each dipping line is migrated at its own CDR velocity $v_{\mathrm{CDR}}$ (see text), rather than at a constant migration velocity. Because of noise-induced variations in $v_{\mathrm{CDR}}$, the reflectors are fuzzy.

However, $v_{\mathrm{CDR}}$ must be used carefully, since it is not stable: it can vary a great deal owing to variations in $p_{\mathrm{s}}$ and $p_{\mathrm{g}}$, especially if the half-offset $h$ is small compared to the depth of the reflector. For instance, a misapplication of $v_{\mathrm{CDR}}$ would be to use it to produce a depth-migrated plot. In theory, of course, $v_{\mathrm{CDR}}$ can be used in place of the a priori velocity $v$ in equations (2.24), (2.25), and (2.26), to produce a depth-migrated plot where each dip bar has been located according to its associated CDR velocity. The problem, as shown in Figure 2.5, is that the variations in $v_{\mathrm{CDR}}$ translate into variations in $z_{\mathrm{R}}$, the migrated depth, in the final plot. These variations in depth lead to a loss of reflector coherency.

There are other types of plots, however, where using $v_{\mathrm{CDR}}$ is entirely appropriate. The main advantage of using $v_{\mathrm{CDR}}$ in producing plots, as will be seen below, is that well-focused plots, including time-migrated sections, can be produced without the need to perform a preliminary velocity analysis. If $v_{\mathrm{CDR}}$ is properly used, the effect is as if a separate velocity analysis were performed for every reflection event. Note, however, that in Soviet practice, $v_{\mathrm{CDR}}$ is not used directly in plotting picked seismic data (Boris Zavalishin,

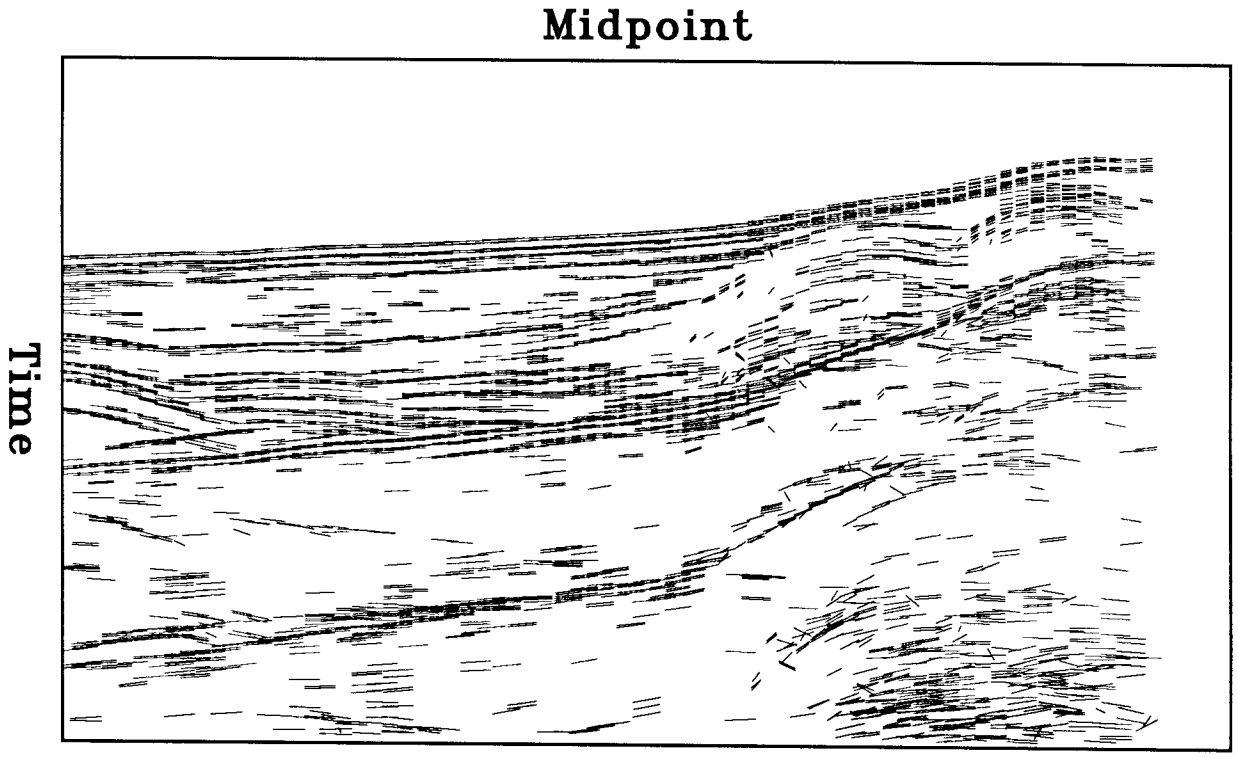


Figure 2.6: CDR simulated stacked section ($v = v_{\mathrm{CDR}}$). Picked parameters from the British Petroleum marine data set are used. Only a normal-moveout correction has been applied to the picked parameters. This normal-moveout correction is based on the value of the CDR velocity $v_{\mathrm{CDR}}$ associated with each dip bar. The reflectors in this figure are much less fuzzy than in Figure 2.5; the main reason is that the dip bars are plotted with a vertical axis that represents time rather than depth.

personal communication); the reason is that it is considered too noise-sensitive for such a purpose. Instead, it is used only in filtering and in performing velocity analyses. The results of the smoothed velocity analyses are used, in turn, to migrate and plot the CDR data.

### CDR simulated stacking

An example of the appropriate use of $v_{\mathrm{CDR}}$ is in producing a simulated stacked section. A simulated stacked section is supposed to reproduce the effects of stacking conventional normal-moveout-corrected seismic data. The simulated stacked section is produced by determining, for each set of picked reciprocal parameters, the plotting parameters $p_{\mathrm{y}_0}$ (the apparent dip of the reflecting segment), $y_{\mathrm{R}}$ (the midpoint location of the reflecting segment), and $t_{\mathrm{R}}$ (the moveout-corrected traveltime to the reflecting segment). These

plotting parameters are found according to the formulas

$$y_{\mathrm{R}} = y, \tag{2.30}$$

$$t_{\mathrm{R}} = \sqrt{t^2 - \frac{4h^2}{v_{\mathrm{CDR}}^2}}, \tag{2.31}$$

and

$$p_{\mathrm{y_0}} = \frac{1}{t_{\mathrm{R}}}\left[t(p_{\mathrm{s}} + p_{\mathrm{g}}) - \frac{4h}{v_{\mathrm{CDR}}^2}\right], \tag{2.32}$$

where $h$ is the half-offset, defined in equation (2.5), and $y$ is the midpoint, defined in equation (2.6). The derivation of equation (2.30) is obvious (the midpoint is unchanged after a simple normal-moveout correction). Equations (2.31) and (2.32) are derived in a fashion analogous to the derivation of equations (2.16) and (2.20). Figure 2.6 shows the result of plotting such a simulated stacked section. The jitter is much less obvious than in Figure 2.5; this is a consequence of remaining in the traveltime domain rather than converting to depth.

### CDR time migration

It has been seen that for simulated stacked sections, the CDR velocity $v_{\mathrm{CDR}}$ can be used successfully to image data, so long as a time-to-depth conversion is not made. This result suggests that time migration might be more successful than depth migration in taking advantage of $v_{\mathrm{CDR}}$. To carry out such a time migration, equations (2.24), (2.25), and (2.26) are used (with $v_{\mathrm{CDR}}$ instead of an a priori $v$) to determine the quantities $\tan\phi$, $y_{\mathrm{R}}$, and $z_{\mathrm{R}}$. Then, a simple depth-to-time conversion converts $z_{\mathrm{R}}$ into the time domain:

$$t_{\mathrm{R}} = \frac{2z_{\mathrm{R}}}{v_{\mathrm{CDR}}}. \tag{2.33}$$

A similar formula converts $\tan\phi$:

$$p_{\mathrm{y_0}} = \frac{2}{v_{\mathrm{CDR}}}\tan\phi. \tag{2.34}$$

The plotting parameters $y_{\mathrm{R}}$, $t_{\mathrm{R}}$, and $p_{\mathrm{y_0}}$ tell where, and with what apparent dip, the time-migrated reflector segment should be plotted. An example of such a time migration is shown in Figure 2.7.

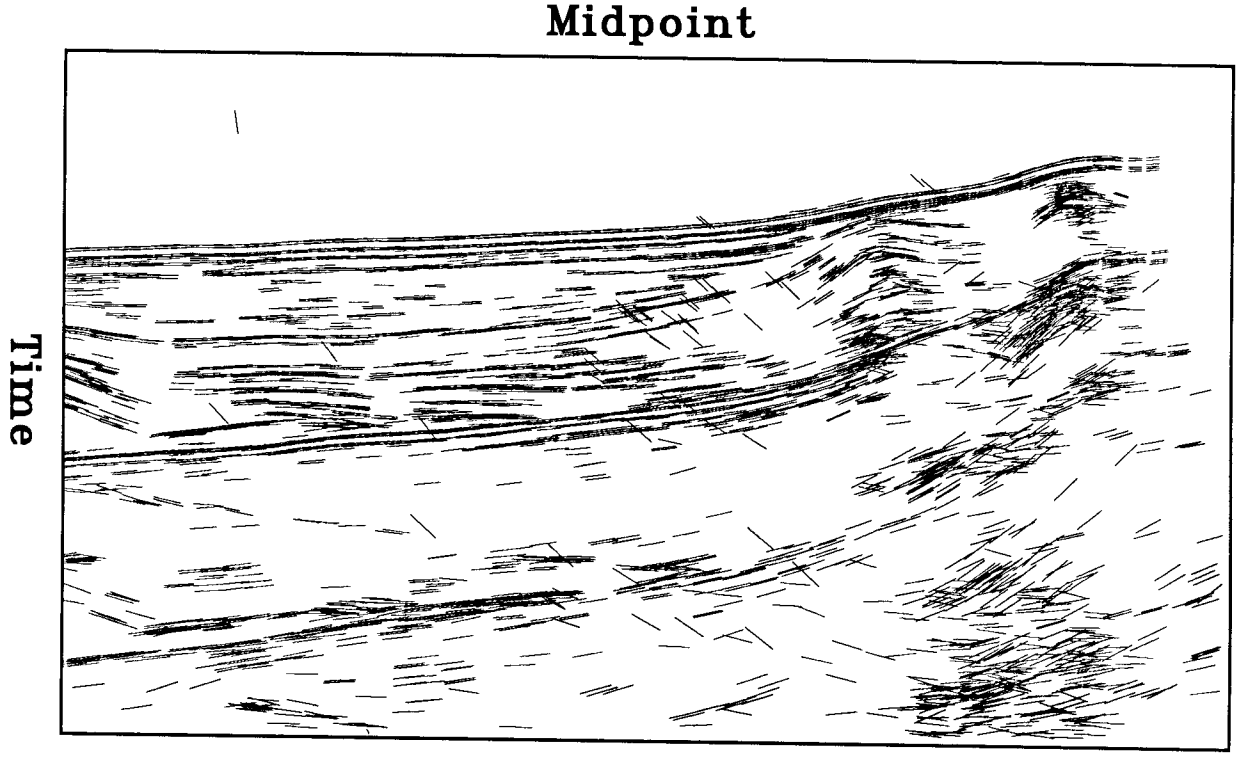


Figure 2.7: CDR migrated time section ($v = v_{\rm CDR}$). The picked British Petroleum marine data have been time migrated, with each dip bar migrated according to its associated CDR velocity $v_{\rm CDR}$. The reflectors are much less fuzzy than in the depth migration in Figure 2.5; the main reason is that the vertical axis in the plot now represents time rather than depth, so that fluctuations in $v_{\rm CDR}$ only lead to small vertical fluctuations in the positions of the dip bars.

### Stereo velocity displays

The CDR velocity $v_{\rm CDR}$ can serve as extra information for the interpreter, if a way can be found to display it. One interesting technique is to display $v_{\rm CDR}$ in the third dimension, allowing depth into the plotted section to be proportional to the measured CDR velocity. I construct such displays by using simple stereo techniques. Two images are plotted: one is plotted normally, and the other is plotted with each dip bar shifted to the right (or left) by an amount proportional to the associated value of $v_{\rm CDR}$. Such a stereo plot is shown in Figure 2.8. Note that the water-bottom multiples, all of which have a $v_{\rm CDR}$ of about 1.5 km/sec, stand out clearly from the higher-velocity primary reflections.

Even more information can be put onto a single plot. For example, the stereo display in Figure 2.9 shows how $v_{\rm CDR}$ varies with offset. It is identical to Figure 2.8, except that each dip bar has been replaced by a letter of the alphabet. Earlier letters (A, B, C, etc.)

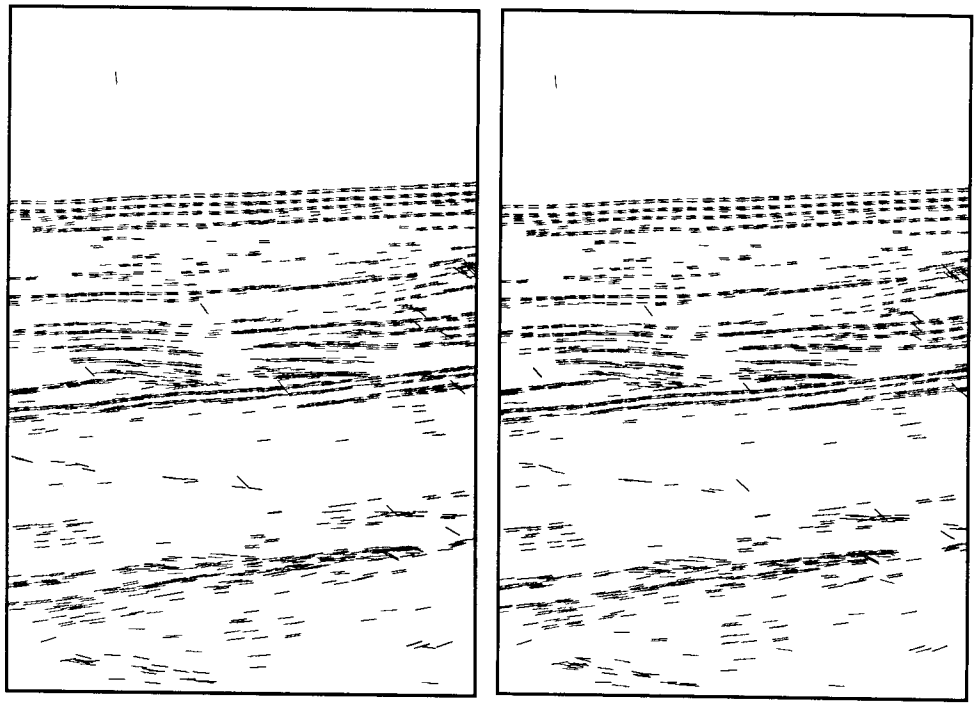


Figure 2.8: Stereo pair. Diagram (b) is an expanded portion of Figure 2.7 (a CDR time-migrated section). Diagram (a) is similar, except that each dip bar has been shifted to the right in proportion to the associated value of $v_{\mathrm{CDR}}$. The result is a stereo plot. Viewed with a stereo viewer or with crossed eyes, an illusion of depth is created, with $v_{\mathrm{CDR}}$ as the third dimension. The water-bottom reflection and its multiples all have low velocities, causing them to stand out from the higher-velocity primary reflections.

replace near-offset dip bars (dip bars whose reciprocal parameters were measured for $x_s$ close to $x_g$), while later letters (R, S, T, etc.) replace far-offset dip bars. Such displays should be used with caution; they may overwhelm rather than aid the interpreter.

## 2.4 Picking field data

Figures 2.4 through 2.9 were constructed using picked data from a British Petroleum seismic survey off Southern California; Paul Fowler provided invaluable assistance in pre-processing these data. This marine data set was used to test the CDR picking program that I developed, and (as will be seen in Chapter 4) to test the method of tomographic inversion.

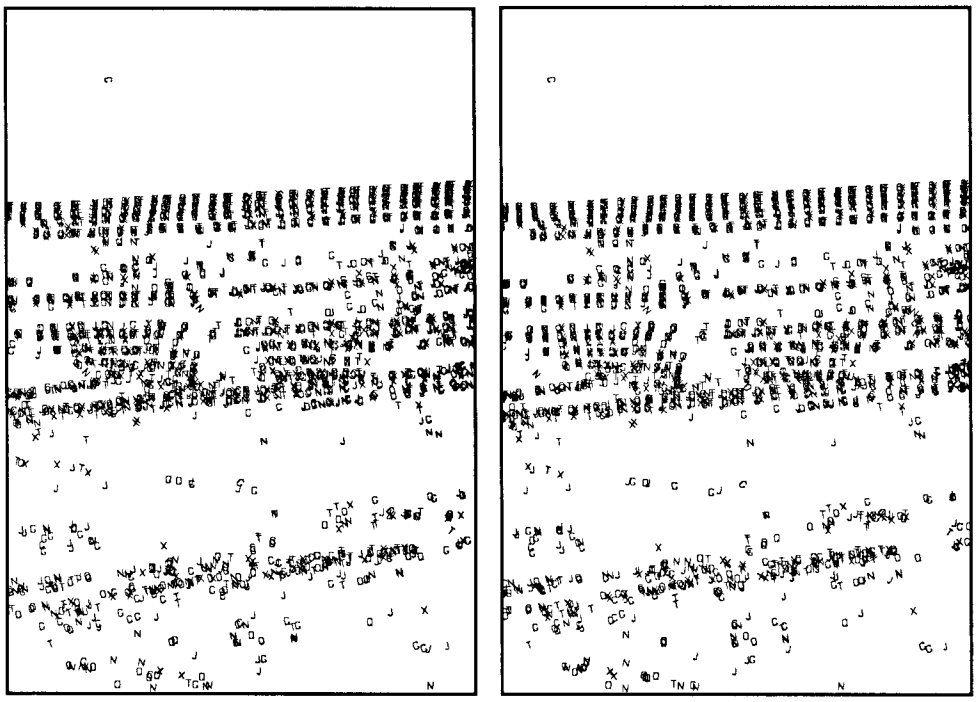

(a) (b)

Figure 2.9: A more complicated stereo plot. This figure is identical to Figure 2.8, except that the dip bars have been replaced by letters of the alphabet. Letters close to A represent dip bars recorded at near offsets ($x_s$ near $x_g$); letters closer to Z represent dip bars recorded at far offsets.

The distance between shotpoints was originally 8.3 meters; I threw out every other shot profile, so the shotpoint spacing became 16.6 meters. The geophone spacing was 33.3 meters. A near-offset section (Figure 2.10) shows that the data were of high quality. The details of the picking process are given in Appendix A. As a result of the picking, 6,507 sets of picked parameters were found.

### 2.4.1 Comparison of picked data to the original section

It is useful to compare how well the picked marine data correspond to the original, unpicked data. This is best done by converting the CDR simulated stacked section (Figure 2.6) from a line drawing to a conventional plot, as in Figure 2.11. To make this plot, picked amplitude information was used in addition to the five reciprocal parameters. This section can be compared to a near-offset section from the unpicked data (Figure 2.10). Such a

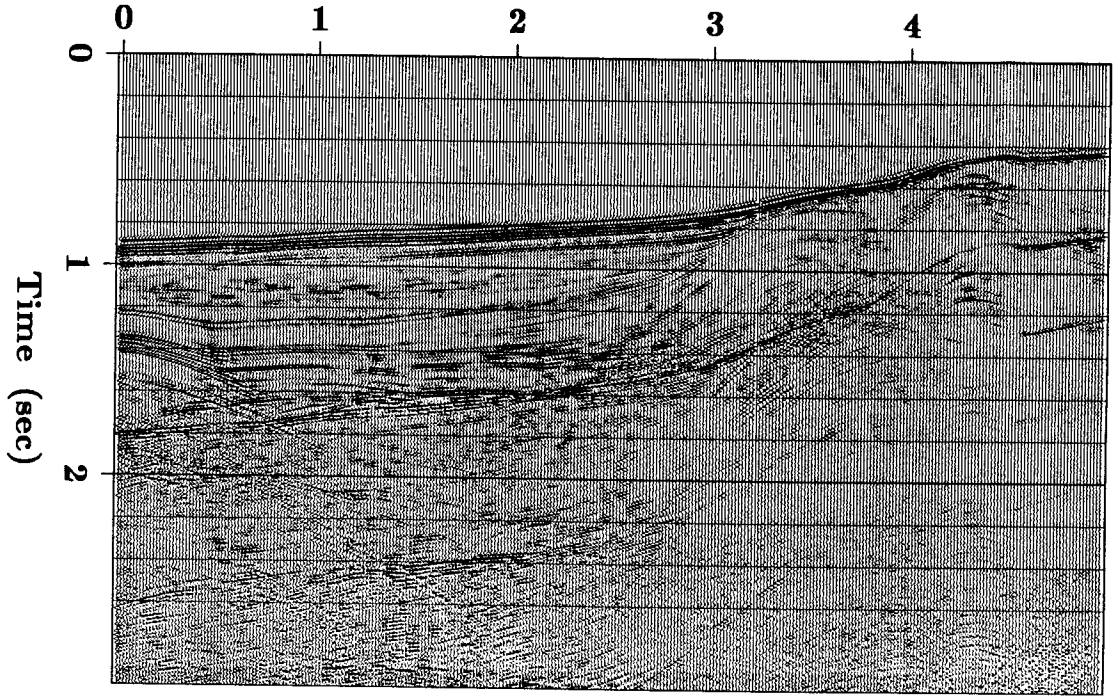


Figure 2.10: Conventional plot of near-offset seismic data. This figure shows the original British Petroleum marine data before picking; the horizontal scale is in kilometers. The only processing that has been applied is a time-dependent gain.

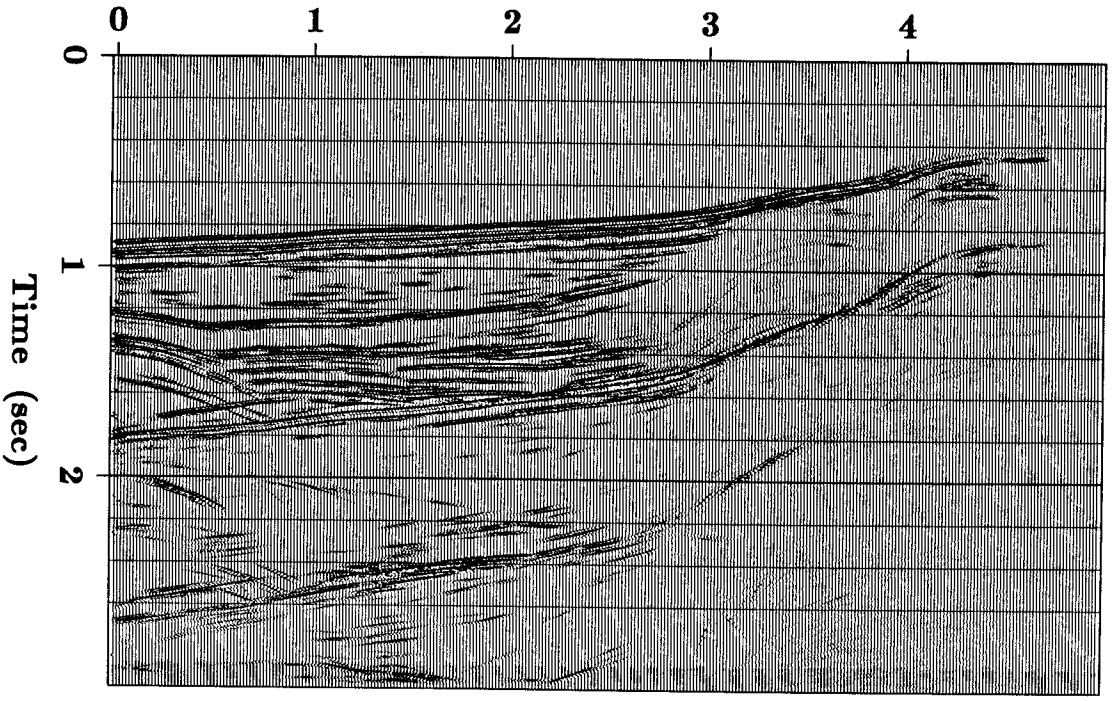


Figure 2.11: CDR simulated stacked section (conventional plot). This, like Figure 2.6, is a simulated stacked section, but the dip bars have been plotted in a more conventional format. A comparison with Figure 2.10 shows the accuracy of the CDR picking procedure.

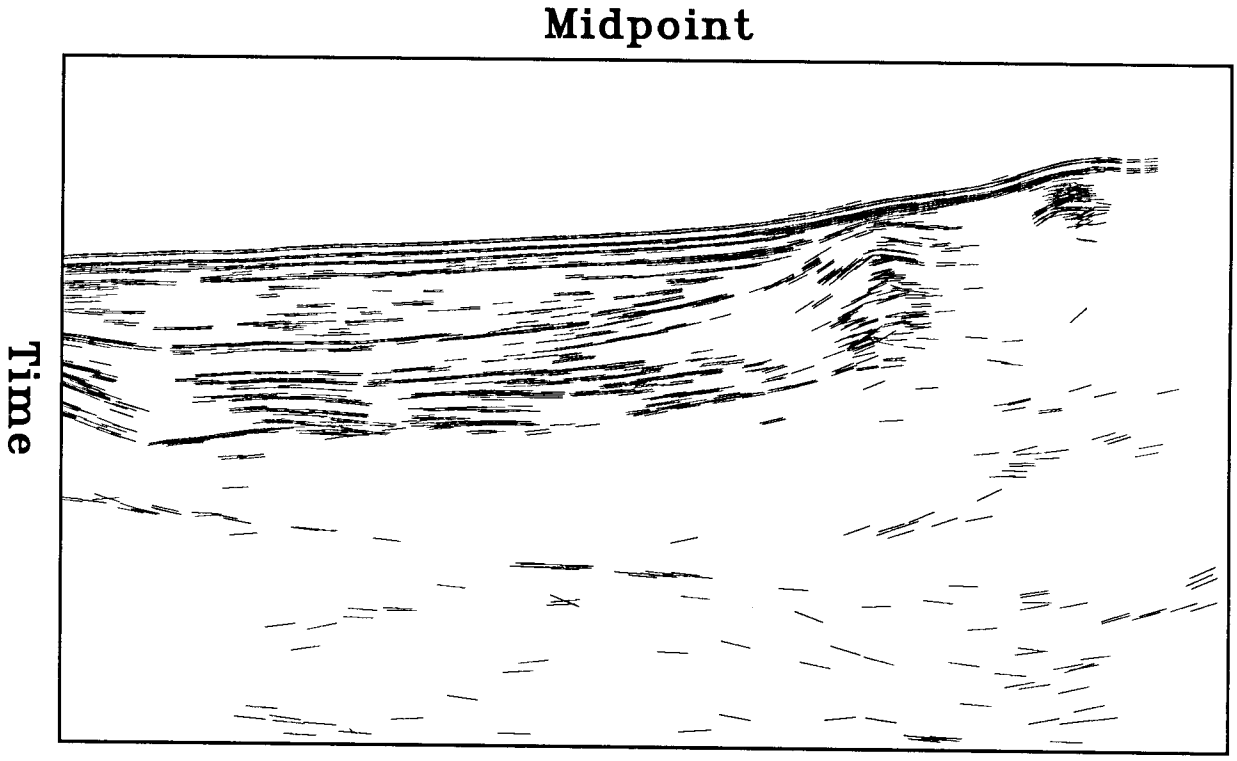


Figure 2.12: Filtered migrated time section. These are the same data, plotted in the same way, as in Figure 2.7, except that undesirable events (such as multiple reflections) have been filtered out on the basis of amplitude, CDR velocity, and dip. Note the deep dipping reflector that is now visible. Note also that the second water-bottom multiple has not been completely eliminated.

comparison shows that the picking process was successful in detecting most major events, without picking too many spurious events (noise).

### 2.4.2 Velocity and amplitude filtering

It will be seen in Chapter 3 that CDR tomographic inversion is not able to deal intelligently with multiples. It is desirable, then, to filter out multiple reflections, and other noise as well, before beginning the inversion process. This filtering is most easily done on the basis of CDR velocity $v_{\mathrm{CDR}}$ (Zavalishin et al., 1982). The filtering process requires some assistance from an interpreter, who must specify which values of $v_{\mathrm{CDR}}$ are acceptable at a given traveltime and midpoint. The main difficulty with velocity filtering is that when depth is large with respect to offset, the value $v_{\mathrm{CDR}}$ is not accurately determined. Owing to this inaccuracy, picks from spurious events such as multiples can appear to have "reasonable" velocities.

Another useful technique for dealing with spurious data is amplitude filtering. When the five reciprocal parameters are picked, amplitude is usually picked as well; an anomalously low amplitude suggests that the associated reflection event is weak or spurious. Such low-amplitude events can usually be rejected.

Figure 2.12 shows a time-migrated section, analogous to Figure 2.7, where many undesirable events have been filtered out on the basis of their anomalous velocity, low amplitude, or anomalous dip.